A comparative study of the polarization degradation mechanisms during electric cycling in $(Bi_{1/2}Na_{1/2})TiO_3$-based relaxors

Zhongming Fan, Xiaoli Tan[a)]

Department of Materials Science and Engineering, Iowa State University, Ames, IA 50011, USA

Abstract

The polarization degradation during electric field cycling in a ferroelectric ceramic is closely related to the phase composition. In the present work, electric biasing *in-situ* transmission electron microscopy (TEM) fatigue tests are conducted on relaxors of $(1-x)(Bi_{1/2}Na_{1/2})TiO_3–xSrTiO_3$. It is directly observed that the ceramic of $x = 0.25$ features an irreversible relaxor-ferroelectric phase transition and the domain walls in the metastable ferroelectric phase sweep shorter and shorter distances during cycling. In contrast, the ceramic of $x = 0.27$ features a reversible relaxor-ferroelectric transition and the domain walls in the transient ferroelectric phase remain highly mobile even after 10^4 cycles.

Keywords: in-situ TEM, electric fatigue, ferroelectric domains, relaxor-ferroelectric transition

[a)]Author to whom correspondence should be addressed. Electronic mail: xtan@iastate.edu

Polarization fatigue, as it can devastatingly affect the device performance, has been regarded as a key issue of ferroelectric ceramics [1,2]. An important research topic is to identify the factors that have critical impacts on their fatigue behavior; these include the external factors such as field amplitude [3], cycling frequency [4], and test temperature [5]. However, factors that are inherent to ferroelectric ceramics are thought to be more crucial. For example, addition of aliovalent dopants and changes in phase compositions can lead to distinct fatigue behaviors in lead zirconate titanate ceramics with similar chemical composition [6,7]. Lead-free piezoelectric ceramics are known to have complex phase transitions in the electric field-temperature space, their phase composition presumably plays a decisive role on their fatigue behavior.

Discussions on the phase composition-fatigue behavior relation have been made in all three major lead-free piezoelectric ceramic systems. In $BaTiO_3$-based ceramics, electric cycling in the orthorhombic phase exhibits a worse fatigue resistance than in the tetragonal phase [8]. In $(K_{0.5}Na_{0.5})NbO_3$-based solid solutions, polarization degradation is considerably mitigated after getting rid of the polymorphic phase transition [9]. In $(Bi_{1/2}Na_{1/2})TiO_3$-based relaxors, a fatigue-free or even anti-fatigue phenomenon is observed when the relaxor-ferroelectric transition is reversible [10-12]. Nevertheless, given the fact that the polarization fatigue is closely related to the domain dynamics under cyclic electric field, experiments that can directly reveal the microstructural evolution during cycling would be more insightful than bulk measurements. In the present study, the electric biasing *in-situ* TEM is employed to compare the different polarization degradation mechanisms in two $(1-x)(Bi_{1/2}Na_{1/2})TiO_3–xSrTiO_3$ (BNST100x, x = 0.25 and 0.27) relaxors [13,14].

BNST25 and BNST27 ceramics were fabricated using the solid-state reaction method, with starting powders of Bi_2O_3 (99.9%), Na_2CO_3 (99.9%), $SrCO_3$ (99.99%) and TiO_2 (99.99%). The

batched powders were mixed in a vibratory mill in ethanol for 6 hours, and dried in oven at 90 °C. Calcination was performed at 850 °C for 2 hours while sintering was carried out at 1100 °C or 1125 °C for 2 hours. The temperature-dependent loss tangent was measured at a heating rate of 4 °C/min using an LCZ meter (Model 3330; Keithley, Cleveland, OH). The polarization hysteresis loops were recorded at 1 Hz using a standardized ferroelectric test system (Precision LC II, Radiant Technologies). For the *in-situ* TEM experiments on a FEI Tecnai G2-F20 microscope, as-sintered pellets were mechanically ground and polished to 120 μm thickness. Disks of 3 mm in diameter were ultrasonically cut and the center portion was thinned to 10 μm by mechanical dimpling. The dimpled disks were annealed at 250 °C for 1 hour to minimize the residual stress before Ar-ion milling until perforation. During the fatigue tests on bulk ceramics and with *in-situ* TEM, cyclic electric fields in a triangular waveform of 1 Hz were applied.

What is the difference between BNST25 and BNST27 in terms of the phase nature? Since BNST25 has been discussed in detail recently [15], Fig. 1 focuses on BNST27 only. In the virgin state (Fig. 1a), the entire grain is occupied with the nanoscale domains. The $[11\bar{2}]_c$ zone-axis diffraction pattern contains two sets of superlattice spots, ½{*ooo*} and ½{*ooe*} type marked by the bright circle and arrow, respectively. It means that, BNST27 is a mixture of the rhombohedral *R3c* phase and the tetragonal *P4bm* phase [16]. Subjected to a voltage of 420 V (Fig. 1b), the nanoscale domains near the top corner of the grain transform into thin tweed-like domains. In the corresponding diffraction pattern, the ½{*ooe*} spots disappear while the ½{*ooo*} spots become more discrete. Such events are interpreted as the field-induced *P4bm* to *R3c* phase transition. Once the voltage is removed (Fig. 1c), not only the domain morphology, but also the diffraction pattern resumes to the initial state, indicating that the phase transition is reversible. On the contrary, BNST25 is known to undergo a field-induced irreversible relaxor-ferroelectric

phase transition and is not accompanied with any change in the crystal structure [15]. In other words, the 2 mol.% more of Sr^{2+} in BNST27 has shifted the depolarization temperature (T_d) down towards room temperature (Fig. 2a); so that the induced long-range ferroelectric order in BNST27 is disrupted upon removal of the field [17,18].

Does a reversible phase transition in BNST27 really correspond to a better fatigue resistance, as similar to other $(Bi_{1/2}Na_{1/2})TiO_3$-based relaxors? As can be seen in Fig. 2b, the polarization-electric field (*P*-*E*) loop of BNST25 changes much more dramatically than that of BNST27 during electric cycling. After 10^4 bipolar cycles at ±40 kV/cm, the maximum polarization ($2P_m$) drops 38% in BNST25 while only 4% in BNST27 (Fig. 2c). On the other hand, the switchable polarization ($2P_r$) decreases by 39% in BNST25 but increases by 5% in BNST27. Note that BNST27 displays a non-zero P_r (Fig. 2c$_2$), indicating the presence of ferroelectric phase. This can traces its origin to the fact that roughly 20% of the grains in BNST27 contain a Sr-deficient core full of lamellar ferroelectric domains [19].

In order to reveal the micromechanism for the strong fatigue resistance in BNST27, *in-situ* TEM fatigue test is conducted on another $[1\bar{1}0]_c$ zone-axis aligned grain (Fig. 3). The reversible relaxor-ferroelectric phase transition takes place in the center of the observed area under 420 V (Fig. 3a-c). After 2×10^3 cycles, the same reversible process is seen (Fig. 3d-f). It should be noted that the cyclic bias of 420 V used here is unipolar. Due to the reversible nature of the phase transition, the responses under +420 V and -420 V are presumably symmetric. So, the unipolar cycling result are presumably able to reflect the bipolar fatigue behavior at some lower cycle numbers, in BNST27. After 10^4 cycles, the tweed-like domains with almost identical appearance can still be induced at 420 V (Fig. 3g-i). Such a stable microstructural response during electric

cycling is perfectly consistent with the excellent fatigue resistance observed in the BNST27 bulk ceramic.

The situation in BNST25 is completely different. In the virgin state, the grain observed along its $[001]_c$ zone-axis is full of nanoscale domains (Fig. 4a). When a voltage of 300 V is applied, the relaxor to ferroelectric phase transition occurs and wedge-shaped large domains form (Fig. 4b) [15]. The long domain walls trace along the $<100>_c$ direction, suggesting that they are very likely on inclined $\{110\}_c$ planes. As the voltage increases, the two major wedge domains grow in size, at the cost of the matrix in between (Fig. 4c). It implies that the wedge domains have the polarization favored by the applied field, while the matrix domain does not. Subsequently, the two long domain walls continue moving toward each other until their middle sections merge (Fig. 4d). The voltage is then removed, but the domain morphology hardly changes (Fig. 4e). Then, the voltage reverses the polarity. The merged domain walls first detach apart (Fig. 4f), followed by the contraction of the two major wedge domains and the growth of the matrix in between (Fig. 4g). After the voltage returns to 0 V from the negative peak value, the domain morphology, again, mostly remains unchanged (Fig. 4h).

Unlike BNST27, the cyclic fields used for the fatigue test in BNST25 are selected to be bipolar rather than unipolar. The reason is that, unipolar fields only lead to the cycling between the remanent state and the poled state in the same polarity ($P_s \approx P_m$ in BNST25), but the severe fatigue degradation is often associated with a more complete polarization reversal process [20,21]. Therefore, the domain switching dynamics is checked after 3×10^3 bipolar cycles at ±420 V. As shown in Fig. 4i, those two major wedge domains are still present at 0 V. Under +420 V, they do grow, but the growth is suppressed, i.e. the long domain walls are no longer able to merge (Fig. 4j). Under -420 V, similarly, the domain wall motion occurs, but it sweeps a shorter

distance (Fig. 4k). Upon the removal of the voltage, the domain morphology at 0 V prior to this checking cycle is restored (Fig. 4l). Apparently, such a suppression of the domain wall mobility in the form of reduced sweeping distance (~210 nm in the fresh state while ~55 nm in the fatigued state) is the fundamental reason for the degradation of ferroelectric properties in the BNST25 ceramic.

What causes the distinctive fatigue behaviors in BNST25 and BNST27? It is well known that oxygen vacancies ($V_O^{\cdot\cdot}$) in pure $(Bi_{1/2}Na_{1/2})TiO_3$ have excellent mobility under high temperature or electric field, which makes it an ideal ionic conductor [22,23]. More importantly, the $V_O^{\cdot\cdot}$ concentration is very sensitive to the aliovalent dopant [24]. Since polarization fatigue is essentially a defect-related phenomenon, particular aliovalent dopants have been found, unsurprisingly, beneficial to the fatigue resistance in $(Bi_{1/2}Na_{1/2})TiO_3$-based ceramics [25-27]. However, the subtle difference in Sr^{2+} concentration, which is equivalent to an isovalent dopant on A-site in the ABO_3 peroskite structure, is unlikely to create an impactful difference in defect concentration between BNST25 and BNST27 [28]. When BNST25 is subject to bipolar cyclic fields, the long walls of the wedge domains sweep back and forth (Fig. 4). It is known that the sidewise motion of domain wall during polarization reversal initiates from a section stepping out from the wall [29]. The head-to-head or tail-to-tail dipole configuration will be formed between the step-out section and the matrix domain [30], giving rise to a local depolarization field (E_d). Usually, E_d is sufficient to overcome the mutual repulsion between point defects of like charge and have them segregated [31,32]. During the continuous sweeping, the long domain walls have numerous opportunities to trap the charged point defects at the E_d sites, and eventually are pinned [21]. In the present TEM experiment, no observable defect clusters are found attaching to

the domain wall in the fatigued state because the domain wall mobility degrades so quickly that the trapped defects do not have enough time to accumulate [33].

In BNST27, there exist at least two main differences. First, the relaxor-ferroelectric phase transition takes place in each and every electric cycle. The ferroelectric phase nucleates from the relaxor phase and the formed relaxor/ferroelectric interface also bears uncompensated E_d. However, the magnitude should be lower than a half of that in BNST25 since the nanoscale domains on the relaxor side do not possess net polarization [34]. As a consequence, the driving force for the defect accumulation is significantly reduced in BNST27. Second, there is no polarization reversal in the induced ferroelectric phase in BNST27. During the reversible relaxor-ferroelectric transition, the induced ferroelectric phase is of transient nature and exists only within a very short period of time when the applied field is in the vicinity of its peak value; it disappears before the unloading is complete. Even if the polarization alignment/domain switching occurs during this transient period [35,36], the defect accumulation process would be interrupted whenever the loading/unloading is below the critical fields. As polarization reversal is essential for fatigue degradation, BNST27 hence exhibits a much stronger degradation resistance. It should be pointed out that BNST27 is not a single relaxor phase at zero field, the ferroelectric phase contributing to the P_r will eventually lead to overall polarization degradation after prolonged electric cycling.

In summary, the correlation between the polarization degradation and the phase transition reversibility in $(Bi_{1/2}Na_{1/2})TiO_3$-based relaxors has been verified. The greater depolarization field generated during the repeating polarization reversal under cyclic fields in the metastable ferroelectric phase accounts for the more severe fatigue degradation in BNST25 where the relaxor-ferroelectric transition is irreversible. In comparison, in BNST27 where the transition is

reversible, no polarization reversal occurs in the transient induced ferroelectric phase and the relaxor/ferroelectric interface exhibits a reduced depolarization field, rendering a much stronger fatigue resistance.

This work was supported by the National Science Foundation (NSF) through Grant DMR-1465254.

[1] X. J. Lou, J. Appl. Phys. 105 (2009) 024101.

[2] D. Lupascu, J. Rödel, Adv. Eng. Mater. 7 (2005) 882-898.

[3] J. Nuffer, D. C. Lupascu, J. Rödel, Acta Mater. 48 (2000) 3783-3794.

[4] N. Zhang, L. Li, Z. Gui, J. Eur. Ceram. Soc. 21 (2001) 677-681.

[5] M. Ozgul, k. Takemura, S. T. McKinstry, C. A. Randall, J. Appl. Phys. 89 (2001) 5100-5106.

[6] K. Amanuma, T, Hase, Y. Miyasaka, Jpn. J. Appl. Phys. 33 (1994) 5211.

[7] Q. Y. Jiang, E. C. Subbarao, L. E. Cross, J. Appl. Phys. 75 (1994) 7433-7443.

[8] Z. Fan, J. Koruza, J. Rödel, X. Tan, Acta Mater. 151 (2018) 253-259.

[9] S. J. Zhang, R. Xia, H. Hao, H. Liu, T. R. Shrout, Appl. Phys. Lett. 92 (2008) 152904/1-3.

[10] Z. Luo, T. Granzow, J. Glaum, W. Jo, J. Rödel, M. Hoffman, J. Am. Ceram. Soc. 94 (2011) 3927-3933.

[11] E. A. Patterson, D. P. Cann, Appl. Phys. Lett. 101 (2012) 042905.

[12] N. Kumar, D. P. Cann, J. Appl. Phys. 114 (2013) 054102.

[13] C. Tian, F. Wang, X. Ye, Y. Xie, T. Wang, Y. Tang, D. Sun, W. Shi, Scr. Mater. 83 (2014) 25-28.

[14] M. Acosta, W. Jo, J. Rödel, J. Am. Ceram. Soc. 97 (2014) 1937-1943.

[15] Z. Fan, X. Tan, Appl. Phys. Lett. 114 (2019) 212901.

[16] R. Beanland, P. A. Thomas, Scr. Mater. 65 (2011) 440-443.

[17] Z. Fan, L. Zhou, T. -K. Kim, J. Zhang, S. -T. Zhang, X. Tan, Phys. Rev. Mater. 3 (2019) 024402.

[18] W. Jo, T. Granzow, E. Aulbach, J. Rödel, D. Damjanovic, J. Appl. Phys. 105 (2009) 094102.

[19] M. Acosta, L. A. Schmitt, L. Molina-Luna, M. C. Scherrer, M. Brilz, K. G. Webber, M. Deluca, H. -J. Kleebe, J. Rödel, W. Donner, J. Am. Ceram. Soc. 98 (2015) 3405-3422.

[20] N. Balke, D. C. Lupascu, T. Granzow, J. Rödel, J. Am. Ceram. Soc. 90 (2007) 1081-1087.

[21] S-H. Baek, C. M. Folkman, J-W. Park, S. Lee, C-W. Bark, T. Tybell, C-B. Eom, Adv. Mater. 23 (2011) 1621-1625.

[22] M. Li, M. J. Pietrowski, R. A. De Souza, H. Zhang, I. M. Reaney, S. N. Cook, J. A. Kilner, D. C. Sinclair, Nat. Mater.13 (2014) 31.

[23] D. Schütz, M. Deluca, W. Krauss, A. Feteira, T. Jackson, K. Reichmann, Adv. Funct. Mater. 22 (2012) 2285-2294.

[24] F. Yang, M. Li, L. Li. P. Wu, E. Pradal-Velázquez, D. C. Sinclair, J. Mater. Chem. A 6 (2018) 5243-5254.

[25] N. Kumar, T. Y. Ansell, D. P. Cann, J. Appl. Phys. 115 (2014) 154104.

[26] J. Shi, W. Tian, X. Liu, H. Fan, J. Am. Ceram. Soc. 100 (2017) 1080-1090.

[27] M. Ehmke, J. Glaum, W. Jo, T. Granzow, J. Rödel, J. Am. Ceram. Soc. 94 (2011) 2473-2478.

[28] H. Zhang, H. Deng, C. Chen, L. Li, D. Lin, X. Li, X. Zhao, H. Luo, J. Yan, Scr. Mater. 75 (2014) 50-53.

[29] R. C. Miller and G. Weinreich, Phys. Rev. 117 (1960) 1460.

[30] Y. -H. Shin, I. Grinberg, I. -W. Chen, A. M. Rappe, Nature 449 (2007) 881.

[31] J. F. Scott and M. Dawber, Appl. Phys. Lett. 76, (2000) 3801-3803.

[32] D. C. Lupascu and U. Rabe, Phys. Rev. Lett. 89, (2002) 187601.

[33] Z. Fan, C. Zhou, X. Ren, X. Tan, Appl. Phys. Lett. 111 (2017) 252902.

[34] X. J. Lou, Appl. Phys. Lett. 94 (2009) 072901.

[35] D. Liu, C. Tian, C. Ma, L. Luo, Y. Tang, T. Wang, W. Shi, D. Sun, F. Wang, Scr. Mater. 123 (2016) 64-68.

[36] E. Dul'kin, E. Mojaev, M. Roth, W. Jo, T. Granzow, Scr. Mater. 60 (2009) 251-253.

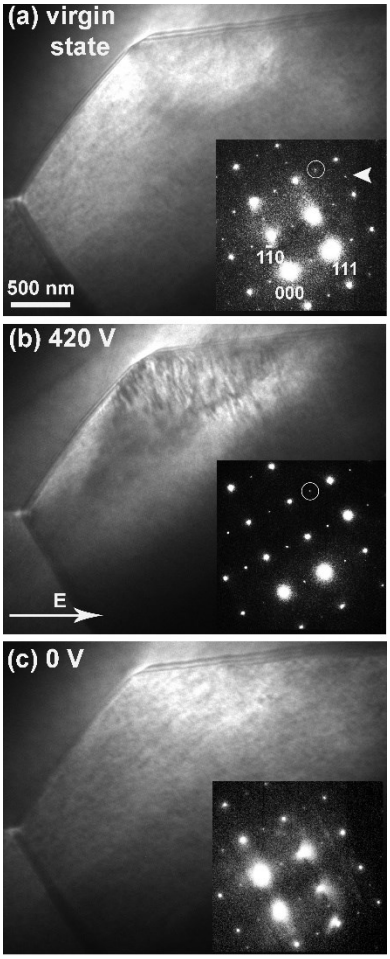

Fig. 1. The reversible relaxor-ferroelectric phase transition in BNST27. TEM bright-field micrographs taken at (a) virgin state, (b) 420 V, (c) 0 V. The insets display the selected area electron diffraction patterns recorded from the top corner of the grain. The bright circles mark the ½{*ooo*} superlattice spots while the bright arrow highlights a ½{*ooe*} spot. The long arrow in (b) indicates the direction of the applied electric field.

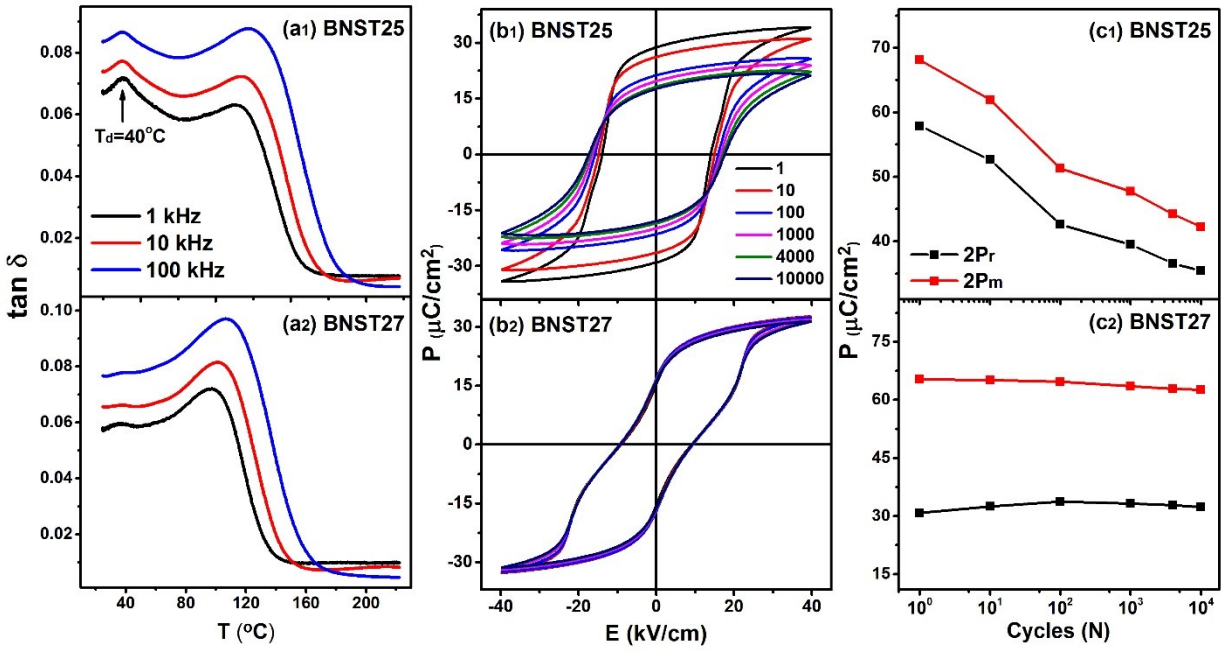

Fig. 2. Electric characterization on bulk ceramic samples. Loss tangent curves measured during heating on poled (a_1) BNST25 and (a_2) BNST27 ceramics. The evolution of the *P*-*E* hysteresis loops during bipolar electric cycling at ± 40 kV/cm in (b_1) BNST25 and (b_2) BNST27 ceramics. (c_1), (c_2) the variation of $2P_m$ and $2P_r$ with cycling number *N*, extracted from (b_1) and (b_2), respectively.

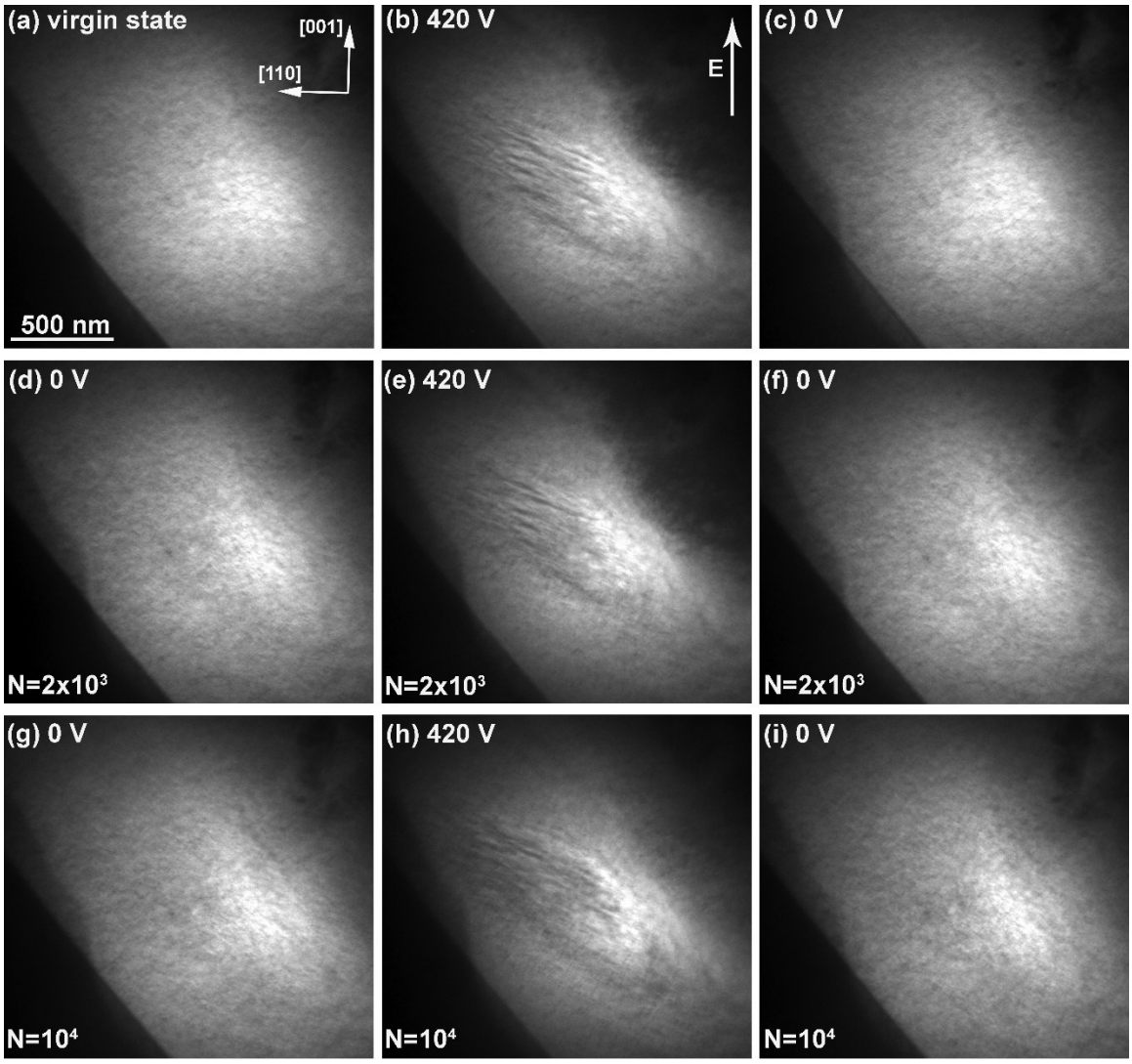

Fig. 3. *In-situ* TEM fatigue test on BNST27. (a)-(c) The microstructural responses in a grain observed along $[1\bar{1}0]_c$ zone-axis during the first unipolar cycle. (d)-(f) The responses after 2×10^3 unipolar cycles at 420V. (g)-(i) The responses after 10^4 unipolar cycles at 420 V. The arrow in (b) represents the direction of the applied/cyclic fields.

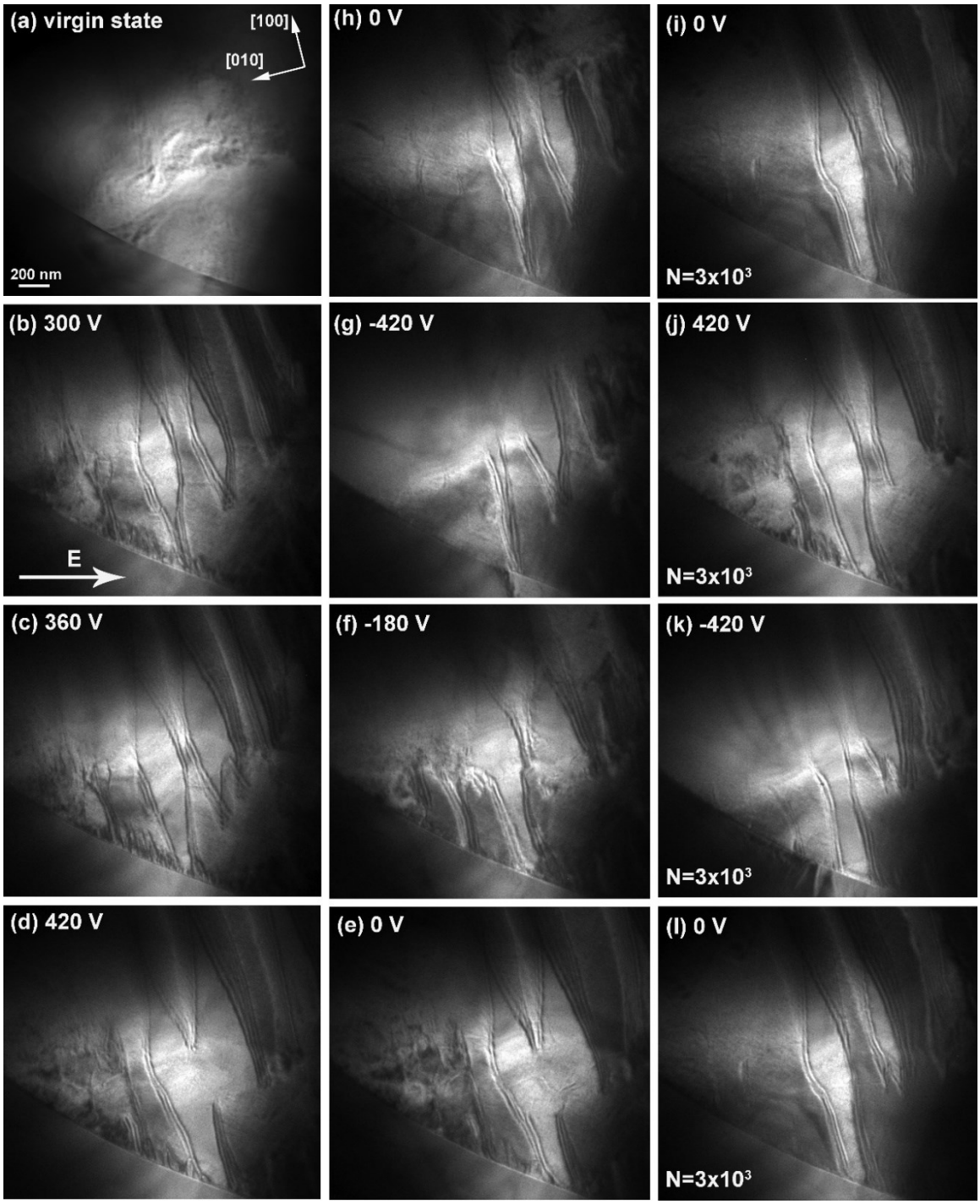

Fig. 4. *In-situ* TEM fatigue test on BNST25. The domain morphology in a $[001]_c$ zone-axis aligned grain at (a) virgin state, (b) 300 V, (c) 360 V, (d) 420 V, (e) 0 V, (f) -180 V, (g) -420 V, (h) 0 V during the first bipolar cycle. The bright arrow in (b) indicates the positive direction of the applied field. (i)-(l) The domain dynamics after 3×10^3 bipolar cycles at ± 420 V.